EPJ Web of Conferences **87**, 02012 (2015)
DOI: 10.1051/epjconf/ 20158702012

High β_p plasma formation using off-axis ECCD in Ohmic heated plasma in the spherical tokamak QUEST

Kishore Mishra[1,a], H. Zushi[2], H. Idei[2], M. Hasegawa[2], K. Hanada[2] and QUEST team

[1] IGSES, Kyushu University, Kasuga, Fukuoka, Japan, 816-8580
[2] RIAM, Kyushu University, Kasuga, Fukuoka, Japan, 816-8580

Abstract. High poloidal beta ($\varepsilon\beta_p$ ~1) operation in steady state condition in tokamaks is of great interest and has previously been demonstrated using NBI, LHCD and low current (I_p) plasma for a short time (<0.5 s). A very few experiments however, have been performed towards the investigation of highest obtainable β_p in tokamak plasma. In this work we report the first result of high β_p production and its sustainment though an off axis ECCD at two different frequencies (fundamental and second harmonic) in Ohmic (OH) target plasma. With application of ECCD, plasma β_p increased to encounter an equilibrium limit and the standard limiter configuration is transformed to an Inboard Poloidal field Null (IPN) configuration. Both off-axis and on-axis ECCD is studied and found to have some distinctive features, which are discussed in this paper.

1 Introduction

Spherical Tokamak is an attractive choice for future fusion reactors for its ability to operate at high poloidal beta ($\beta_p = 2\mu_0\langle p\rangle/\langle B_p\rangle^2$) value. Here $\langle p\rangle = \int p dV$ is volume averaged plasma pressure and $\langle B_p\rangle$ is average poloidal magnetic field over last closed flux surface. Operating a tokamak at high β_p , utilizes a larger fraction of bootstrap current, which may reduce large external current drive requirement and possibly better confinement properties due to modified equilibrium scenarios. For advanced tokamak operational regimes, both normalized beta $\beta_N = \beta_t B_0 a/I_p{}^2$ (for fusion gain performance) and poloidal beta (for bootstrap current) needs to be maximized, subject to the respective MHD equilibrium limits. Here I_p is the driven plasma current having plasma minor radius a and toroidal magnetic field B_0 at the axis. For attaining a high β_p plasma, it is known to utilize an external source to heat the bulk Maxwellian component of the plasma [1,2] or to create a confined anisotropic population of energetic particles[3,4]. It is also proposed to operate in a shaped configuration to increase β_p [5]. High β_p plasma has been produced by injecting multi-megawatt NBI power to Ohmic plasma in different machines [6-8]. The maximum achievable β_p is limited by a so called equilibrium limit, where an Inboard Poloidal field Null (IPN) appears at the high field side of the vacuum vessel. Although it is predicted and studied theoretically in much detail, such an extreme situation is rarely achieved experimentally[8] or it has been found extremely difficult to sustain such equilibrium. The natural IPN configuration is first observed transiently in CDX-U and DIII-D during the current ramp-up and closed flux formation [9] phase, but no measurements are done. In TFTR [8], a null point appeared at the inboard side in high β_p plasma formed by ramping down the plasma current (I_p) in a NBI heated plasma. Such high β_p plasma production and sustainment required > 16 MW of NBI power.

In this paper, we present a scenario of production of high β_p plasma ($\varepsilon\beta_p$ > 1.3) by confining the energetic electrons produced by Electron Cyclotron Waves (ECWs) more flexibly in various operational regime with ECRH/ECCD. The high β_p plasma is kept in equilibrium by suitable vertical magnetic field configuration and is sustained for more than 1 s. As a consequence of high β_p, a natural inboard poloidal null appeared in the vacuum vessel, which moves further into the vacuum vessel as β_p increased beyond 2. Additionally, it is worth mentioning that the high β_p plasma is produced and maintained by injecting a very modest input power of ~100 kW.

The paper is organized as follows. Section 2 describes the experimental conditions and details of the experimental device. In section 3, off-axis ECCD by 8.2 GHz RF in Ohmic plasma is discussed and in section 4 similar experiments with second harmonic 28 GHz ECRH system is presented. Summary of high β_p equilibrium characteristics in both these scenarios are discussed and concluding section outlines the future work.

[a] Corresponding author: mishra@triam.kyushu-u.ac.jp

Article available at http://www.epj-conferences.org or http://dx.doi.org/10.1051/epjconf/20158702012

2 Experimental details

QUEST is a medium sized spherical tokamak [10] with the major and minor radii of 0.68 and 0.4 m, respectively. The center stack (CS), which holds the Ohmic (OH) coil has an outer diameter of 0.2 m and the outer wall of the vacuum vessel is at 1.4 m with the flat divertor plates at z ~ ± 1 m from the mid-plane. Inboard plasma boundary is defined by a limiter on the CS at 0.23 m. QUEST is very well equipped with various sets of Poloidal Field (PF) coils as shown in figure 1. QUEST has unique capability of producing various vertical magnetic field configurations by setting current in different combinations of PF coils. Curvatures of field lines produced due to each coil are different, which holds the key in fast current start up fully non-inductively with ECRH/ECCD. Field lines produced by some combinations of coils are shown in figure 1. Each coil produces different mirror ratio defined as $M=B_{tmax}/B_{tmin}$ on a particular field line originating at mid plane and terminating at vessel wall. It has been demonstrated previously [11] that high M is favorable for fast current start up fully non-inductively by confining energetic electrons produced due to EC waves in QUEST. M is not uniform along radial direction due to different curvature and connection lengths of the field lines produced by different PF coils. Radial variation of M for different PF coils and their combinations are shown in figure 2. Confinement and orbits of energetic electrons should significantly modified due to this non-uniform M and effect of on-axis and off-axis ECCD in this scenario is investigated.

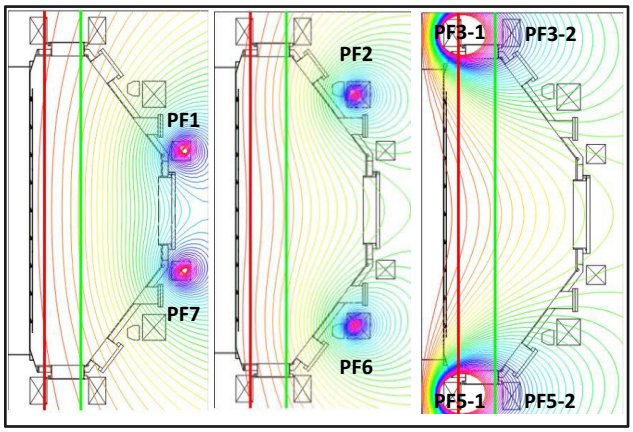

Fig. 1 : Examples of vertical magnetic field lines and their curvatures (poloidal cross section) produced due to different Poloidal Field coils are shown. The coil pairs which are energized for each plot can be easily recognized from the contour plots. The vertical red lines represent fundamental (red) and second harmonic (green) cold electron cyclotron resonance for 8.2 GHz.

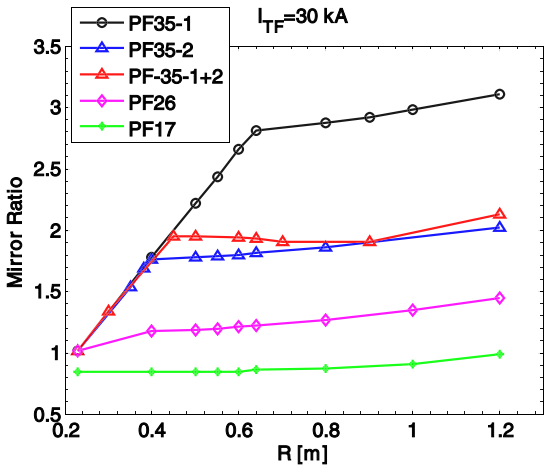

Fig. 2 : Mirror ratios (M) of vertical magnetic field lines as a function of major radius for different combinations of PF coils for a fixed toroidal field (B_t) are shown. The sharp decline in M towards high field side is due to short connection length and higher B_t.

Figure 3 shows toroidal view of QUEST vacuum vessel and various heating systems and diagnostics used in this experiment. Two 8.2 GHz (~ 2 x 8 x 25= 400 kW) Klystrons assemblies are used to inject O and X-mode waves from two separate phased array antennae located at the Low Field Sides (LFS) toroidally 180 degree opposite. While one antenna is phased to inject O-mode waves at n||= 0.4, the other injects mixed modes. These two systems are used to start-up the plasma and later to inject heating pulses with Ohmic plasma. These two systems are used for both off-axis and on-axis fundamental ECCD experiments. Another high power Gyrotron at 28 GHz developed at University of Scuba [12] is used to perform off-axis second harmonic start-up and ECCD experiments.

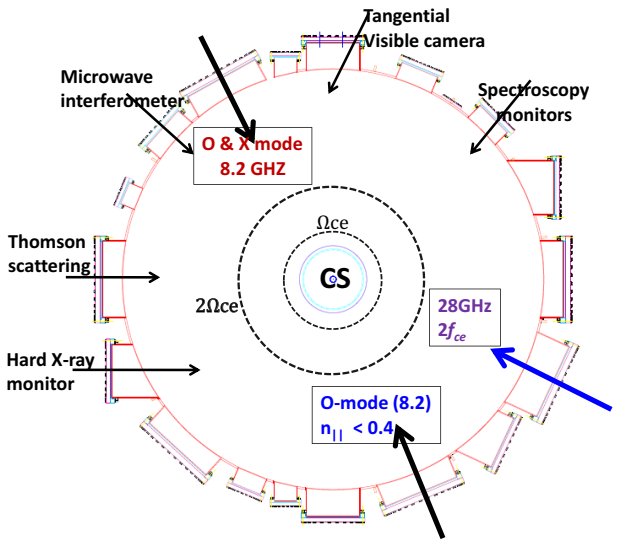

Fig. 3 : Toroidal view of QUEST vacuum vessel showing positions of 8.2 GHz and 28 GHz ECRH systems. Locations of some of the diagnostics are also shown. Locations of fundamental and second harmonic resonances are indicated by broken circles (not to scale).

3 Fundamental off-axis/on-axis ECCD

In case of fully non-inductive current start-up and sustainment with ECW two pair of PF coils, namely PF35-1 and PF35-2 have been used. In the present experiment of ECW heated Ohmic plasma, all four sets of PF coils are used to sustain ECCD plasma current in equilibrium. At first, I_p is initiated by injecting ~ 100 kW of ECW power at 8.2 GHz for 150 ms from the two antennae located at the LFS followed by the OH phase. In the OH phase, I_p is fed back to the OH coil power supply in order to maintain it at -30 kA ± 10%. Here the negative I_p is defined clockwise as seen from the top of the torus. The toroidal field (B_t) is set at 0.29 T at the fundamental resonance R_{fce} = 0.33 m corresponding to off-axis ECCD, where a vertical magnetic field B_z ~ 25 mT is applied. At 2 s of the I_p flattop, another ECW pulse is injected. This results an increase in I_p from -30 kA to -32 kA in 0.3 s (Fig. 4). Due to the feedback circuit, OH coil current (I_{CS}) is reversed transiently to produce a retarding electric field (positive loop voltage V_L) in order to bring back I_p to the feedback value. I_{CS} is shown in fig. 4, is reversed and recharged for a period of 0.2 s. During this time B_z is suitably ramped up to keep plasma in equilibrium without which I_p is not sustained. In similar discharges, strong recharging of OH transformer and ECCD has been earlier observed [13] under certain conditions of equilibrium control in OH plasma. Hard X-ray photons generated due to multiple interaction of ECWs are detected by *CdTe* detector and it shows a substantial increase in

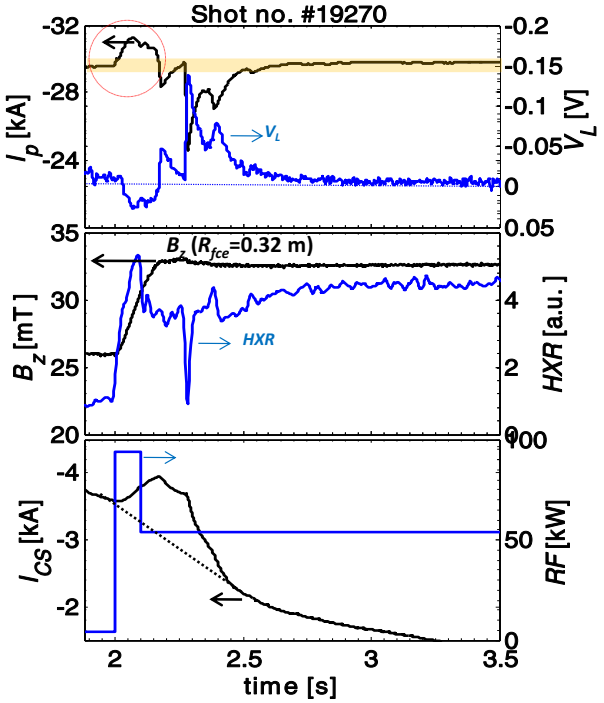

Fig. 4 : Typical Ohmic plasma discharge with I_p feedback operation superimposed with off-axis ECCD pulse. Time traces of I_p, loop voltage (V_L), applied vertical field (B_z), Hard X-ray counts, Ohmic coil current (I_{CS}) and RF pulse are shown. The dotted lines in I_{CS} indicates its decay without the RF injection.

counts as RF is injected. Plasma shape and position are identified by the magnetic measurements from the 64 flux loops outside the plasma. The magnetic flux contours are reconstructed by a fitting procedure described in ref. 14.

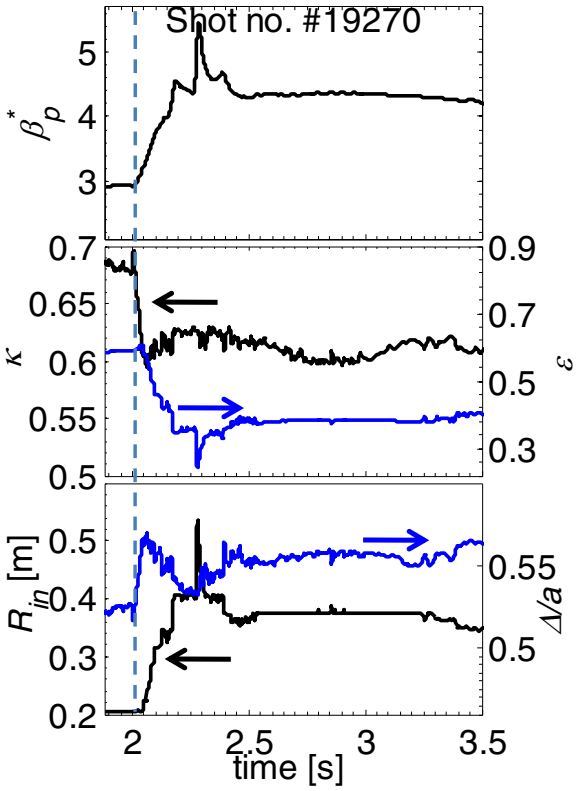

Fig. 5 : Plasma shape (elongation κ and inverse aspect ratio ε) and normalized Shafranov shift (Δ/a) before and after the RF injection is shown. Inboard edge (R_{in}) of plasma shows its shift into the vacuum vessel in ECCD phase creating a natural divertor configuration.

Inboard (R_{in}) and outboard (R_{out}) plasma edges are indentified by this reconstruction and various plasma shape and equilibrium parameters are computed. Figure 5 shows time variations of such parameters in OH and ECRH phases. Plasma elongation ($\kappa = b/a$, b is half minor radius along vertical direction and a is half minor radius along radial direction, a is calculated as (R_{out} - R_{in}) / 2) shows it decrease from 0.7 to 0.6 with RF injection and continues to remain in an oblate shape in the entire RF phase. Similarly inverse aspect ratio ($\varepsilon = a/R_0$, R_0 = (R_{out} + R_{in}) / 2) shows it is reduced from 0.6 during OH phase to 0.4 in RF phase. This shows plasma is shifted outward and becomes oblate shape. Consequently R_{in} shows it is detached from the limiter ($R_{limiter}$ = 0.22 m) shortly after RF is injected and continues to move inside the vacuum chamber up to R = 0.4 m. This is an indication of formation of a natural inboard divertor and suggests an appearance of poloidal field null point inside the vessel.

This is confirmed by tangential visible camera images taken from outboard side as shown in figure 6. Two distinct spots of maximum light intensity can be clearly seen on the inboard CS, which suggests locations of separatrix strike points. The poloidal magnetic flux contours determined from fitting method are superimposed on the image. They fairly agrees with the bright spots seen on the CS, confirming natural separatrix formation. The poloidal field null point is same as measured R_{in} shown in figure 5. This clearly suggests that plasma configuration is transformed from inboard limiter bounded (OH phase) to a natural separatrix bounded IPN configuration (RF phase). This transformation is a consequence of high β_p formation.

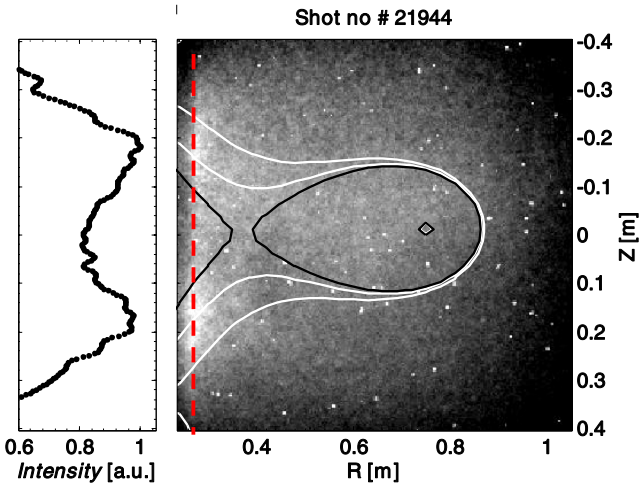

Fig. 6 : Visible camera image of a similar shot shows two distinct bright spots on inboard CS corresponding to separatrix strike points. Reconstructed magnetic flux contours overlaid on the image also shown. Intensity along vertical broken line shows two distinctive peaks.

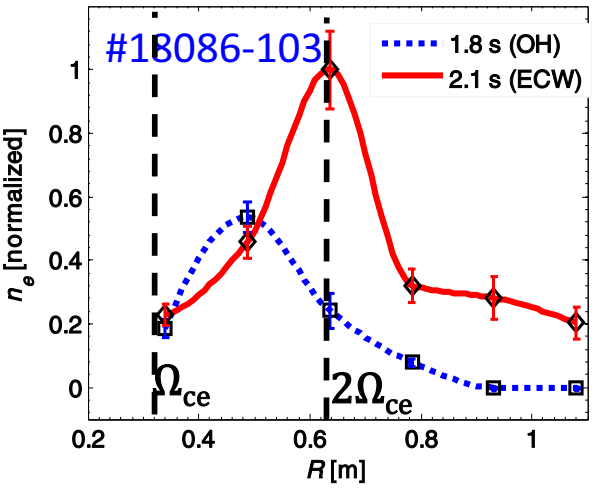

Fig. 7 : Density profile before and after the RF injection in similar discharges shows outward shift of its peak indicating high β_p formation. The fundamental and second harmonic cold resonances are indicated by the broken lines.

We evaluate β_p from the generalized Shafranov equation for radial force balance for the equilibrium vertical magnetic field [15]

$$B_z = \frac{\epsilon B_\theta(a)}{2}\left[ln\frac{8R_0}{a} + \beta_p + \frac{l_i}{2} - \frac{3}{2}\right], \quad (1)$$

where $B_\theta(a) = \mu_0 I_p / 2\pi a$ is the poloidal magnetic field at the boundary $r = a$. l_i is the internal inductance assumed here to be unity and not varying. $\beta_p^* = \beta_p + l_i/2$ evaluated from this method shows that it started increasing from 3 during OH phase to over 5 in RF phase. The spike at 2.3 s is due to a minor disruption in I_p. There is very good correlation between β_p^* and resulting R_{in}. Another signature of this enhancement can be seen from large Shafranov shift (Δ/a) during RF injection as shown in figure 5. The density centroid is also shifted outward during RF phase as measured by Thomson Scattering diagnostic (figure 7). The shift is agreed well by the flux loop measurement and interestingly coincides with second harmonic resonance location. Similar experiments are carried out with higher B_t with on-axis heating (R_{fce} = 0.54 m), however, response of RF on I_p and β_p are considerably reduced. This situation is shown in the following section.

4 Second harmonic off-axis ECCD

Similar experiments as discussed above, is performed with a 28 GHz Gyrotron system installed on QUEST. TF coil current is set at 50 kA corresponding to R_{2fce} = 0.32 m for second harmonic ECCD. This is again off-axis with ~ 100 kW of 8.2 GHz on-axis ECCD pulse is

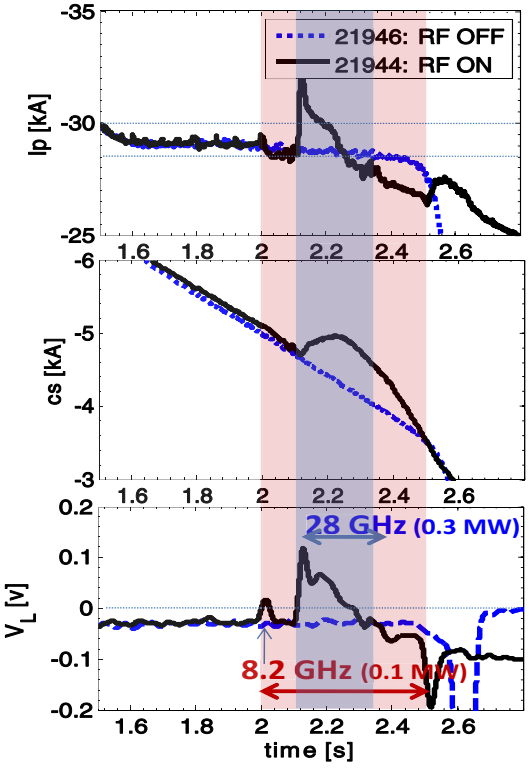

Fig. 8 : Time traces of plasma current (I_p), Ohmic coil current (I_{cs}) and loop voltage shown for Ohmic plasma

with superimposed 8.2 GHz and 28 GHz ECCD pulses. Two similar discharges with and without RF are shown.

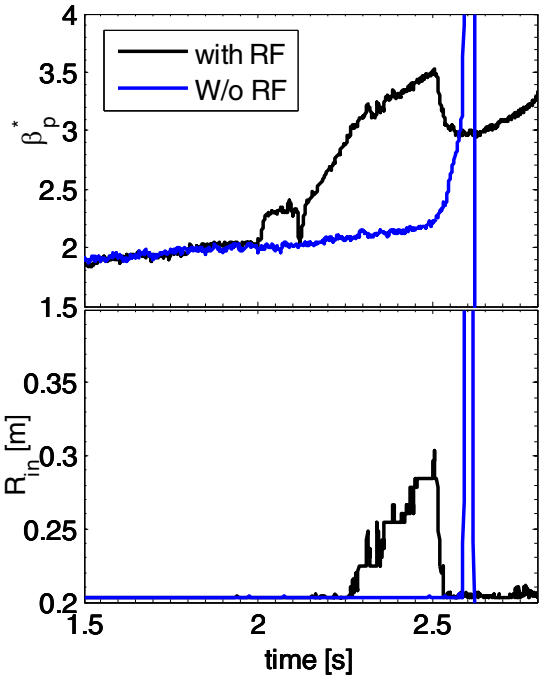

Fig. 9 : Time traces of plasma current (I_p), Ohmic coil current (I_{cs}) and loop voltage shown for a typical Ohmic plasma with superimposed.

similar position to that in 8.2 GHz fundamental ECCD case. Ohmic target plasma is created with I_p = -30 kA applied at t = 2.0 s. Unlike the off-axis case as discussed in the previous section, in the on-axis ECCD, the recharging of OH circuit is comparatively small. Figure 8 shows that V_L is marginally reversed at 2 s without any appreciable enhancement of I_p. However, with application of 28 GHz (~ 300 kW) off-axis ECCD to this plasma, significant recharging of OH circuit and reversal of V_L is observed. I_p is sustained for < 0.2 s believed to be limited by the available pulse length. Figure 9 shows the measured β_p^* and R_{in} position for the above discharges. It can be seen that although β_p^* is marginally enhanced with on-axis ECCD at 2 s, no change in configuration is observed. However, with off-axis ECCD with 28 GHz pulse, β_p^* increased dramatically and IPN configuration is realized after 2.2 s. It may be noted that the enhancement of β_p^* in this case is also partially contributed by decreasing I_p, thus B_p.

5 High β_p and formation of IPN

Figure 10 summarizes β_p^* with I_p and R_{in} for the above discharges. For off-axis ECCD, clearly β_p^* could be raised at constant I_p, however, for on-axis ECCD cases high β_p could not be sustained at high I_p. Fig. 10(a) clearly shows two distinct relationships for on-axis and off-axis ECCD cases. This difference in observations may be attributed to non-uniform M (fig. 2) for on and off-axis ECCD cases owing to difference in confinement orbits of trapped energetic particles in the magnetic field. The detailed mechanism is under investigation and will be reported separately. Nevertheless, the Inboard Limiter (IL) to IPN configuration transition shows very similar results for both the scenarios. IL to IPN transition occurs where R_{null} > 0.22 m, corresponds to β_p^* ~ 3. R_{null} moves almost linearly towards outboard with β_p^*. Such critical values of β_p^* for configuration change has been addressed [16] successfully with an simple analytic model for high β_p spherical torus configuration. The IPN configuration has few other striking features making it worth investigating, which are beyond the scope of this paper at present and will be separately reported shortly.

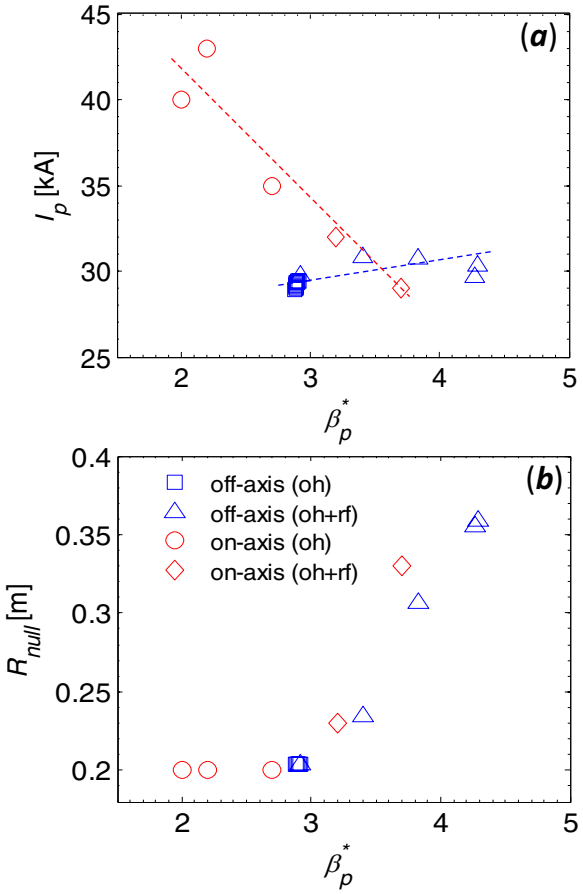

Fig. 10 : (a) I_p ~β_p^* relationship for OH + RF discharges are shown. Broken lines (guidelines) are showing two distinct relationships for off-axis and on-axis ECCD. (b) R_{in} (= R_{null}) dependence on β_p^* shows a transition from inboard limiter to IPN configuration for β_p^* > 3 for all the above discharges.

6 Conclusion

High β_p plasma is produced in Ohmic plasma by off-axis fundamental and second harmonic ECCD at two different frequencies separately. With high β_p plasma undergone a change in configuration as it approaches equilibrium limit. It changes from an inboard limiter in Ohmic phase to naturally created IPN configuration. On axis ECCD however, is found to be not as effective as the off-axis case. β_p and I_p relationships are found to be

distinctively different in both the cases. In both the cases, a critical β_p is found to exist beyond which, plasma equilibrium takes IPN configuration. Role of energetic particle confinement in both these cases is being studied as a future work.

Acknowledgement

This work is supported by Grant-in-aid for Scientific Research (S24226020, A21246139). This work is also performed with the support and under the auspices of the NIFS Collaboration Research Program (NIFS11KUTR063).

References

1. D. W. Swain, Nucl. Fusion 21, 1409 (1981)
2. T. C. Simonen et. al., PRL 61, 1720 (1988)
3. S. C. Luckhardt et. al., PRL 62, 1508 (1989)
4. T. Maekawa et. al., Nucl. Fusion 31, 1394 (1991)
5. J. P. Freidberg, RMP 54, 834 (1982)
6. Y. Koide et. al., Phy. Rev. Lett. 72, 3662, (1994)
7. S. Ishida, Y. Koide, T. Ozeki, M. Kikuchi, S. Tsuji, H. Shirai, O. Naito, and M. Azumi, Phy. Rev. Lett. 68, 1531, (1992)
8. S. A. Sabbagh *et. al*., Phys. of Fluids **B3**, 2277 (1991).
9. C. B. Forest *et. al*. Phys. of Plasma **1**-5, 1568 (1994).
10. K. Hanada *et al*., Plasma Fusion Res. **5**, S1007 (2010).
11. S. Tashima et. al. Nucl. Fusion **54**, 023010 (2014)
12. R. Minami et. al. Nucl. Fusion **53**, 063003 (2013)
13. Kishore Mishra et. al. JPS Conf. Proc. , **015031** (2014)
14. M. Hasegawa et al., IEEJ Trans.FM **132**, 477 (2012)
15. J. P. Freidberg, Ideal Magnetohydrodynamics, Plenum Press, New York, (1987)
16. Kishore Mishra et. al. Plasma Fusion research, Volume **9**, 3402093 (2014)